

Growth and properties of oxygen- and ion-doped $\text{Bi}_2\text{Sr}_2\text{CaCu}_2\text{O}_{8+\delta}$ single crystals

D. B. Mitzi, L. W. Lombardo, and A. Kapitulnik

Department of Applied Physics, Stanford University, Stanford, California 94305

S. S. Laderman and R. D. Jacowitz

Circuit Technology Research and Development, Hewlett-Packard Company, 3500 Deer Creek Road, Palo Alto, California 94304

(Received 29 August 1989)

A directional solidification method for growing large single crystals in the $\text{Bi}_2\text{Sr}_2\text{CaCu}_2\text{O}_{8+\delta}$ system is reported. Ion doping, with replacement of La for Sr and Y for Ca, as well as oxygen doping in these crystals has been explored. Doped and undoped crystals have been characterized using microprobe analysis, x-ray diffraction, thermogravimetric analysis, and magnetic and Hall measurements. Ion doping results in little change of the superconducting transition for substitution levels below 20–25%, while beyond this level the Meissner signal broadens and the low-temperature Meissner signal decreases. Microprobe analysis and x-ray diffraction performed on these more highly substituted single crystals provide evidence for inhomogeneity and phase segregation into regions of distinct composition. Annealing unsubstituted crystals in increasing partial pressures of oxygen reversibly depresses the superconducting transition temperature from 90 (as made) to 77 K (oxygen pressure annealed), while the carrier concentrations, as determined from Hall effect measurements, increase from $n = 3.1(3) \times 10^{21} \text{ cm}^{-3}$ (0.34 holes per Cu site) to $4.6(3) \times 10^{21} \text{ cm}^{-3}$ (0.50 holes per Cu site). No degradation of the Meissner transition or other indications of inhomogeneity or phase segregation with doping are noted, suggesting that oxygen-doped $\text{Bi}_2\text{Sr}_2\text{CaCu}_2\text{O}_{8+\delta}$ is a suitable system for pursuing doping studies. The decrease in T_c with concentration for $0.34 \leq n \leq 0.50$ indicates that a high-carrier-concentration regime exists in which T_c decreases with n and suggests that this decrease does not arise from material inhomogeneity or other materials problems. An examination of the variation of T_c with the density of states and lattice constants for all of the doped and undoped superconducting samples considered here indicates that changes in T_c with doping are primarily affected by changes in the density of states (or carrier concentration) rather than by structural variation induced by the doping.

I. INTRODUCTION

The ability to examine superconducting and normal-state properties as a function of carrier concentration is an important experimental probe of the cuprate high-temperature superconductors. Control over carrier concentration is typically achieved by substituting ions with different preferred valence states on lattice sites around the covalently bonded Cu—O sheets or by annealing in atmospheres with controlled oxygen partial pressures to alter oxygen site occupancy in the structure. These modifications are often referred to as “doping” since the number of carriers is expected to be altered. Common ionic substitutions include La^{3+} for Ba^{2+} in $\text{LaBa}_2\text{Cu}_3\text{O}_{7-\delta}$,^{1–5} and Sr^{2+} for La^{3+} in $\text{La}_2\text{CuO}_{4-\delta}$,^{6,7} $\text{YBa}_2\text{Cu}_3\text{O}_{7-\delta}$, $0 \leq \delta \leq 1$, with its oxygen deficient Cu—O “chain layer,” is the most notable example of carrier concentration controlled through sample oxygen content.

Key to all “doping” experiments is the assumption that ionic substitutions or oxygen site vacancies occur homogeneously throughout the sample and that a continuous range exists over which the carrier concentration can be varied using substitutions or annealing. Homogeneity is particularly critical for the cuprate high-temperature superconductors given the small coherence length in these

materials.

Recently, several groups have prepared and examined ceramic Y^{3+} (Refs. 8–17) and La^{3+} (Ref. 18) substituted



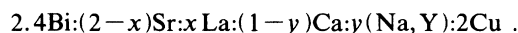
samples. The consistent variation of the lattice constants with substitution^{8–11,18} demonstrates that, in fact, Y and La substitute over a fairly broad range of stoichiometries. However, in some studies the superconducting transition temperature appears to be insensitive to small substitution levels of Y^{3+} for Ca^{2+} ,^{8,9} with an abrupt disappearance of superconductivity above this level. In other studies, the superconducting transition temperature appears to diminish continuously with substitution.^{11,12} In either case, the Meissner transition degrades consistently with substitution level, as has been observed in other “doped” ceramic superconductors,⁶ suggesting sample inhomogeneity, at least on a microscopic scale.¹⁹ Conflicting reports over whether the oxygen content remains relatively fixed⁹ or varies over a large range ($0.1 \leq \delta \leq 0.5$) (Refs. 11 and 18) upon annealing or substitution of a 2+ ion with a 3+ ion must also be examined in order to establish the role oxygen stoichiometry plays in determining carrier concentration.

Given the large anisotropy in the $\text{Bi}_2\text{Sr}_2\text{CaCu}_2\text{O}_{8+\delta}$ system and the potential for inhomogeneity, single crystals are clearly the most instructive medium in which to examine the questions raised by the ceramic samples and to further address the effect of ion substitutions and oxygen intercalation on the high-temperature superconductors. In this study we report on the synthesis and characterization of Y- and La-substituted $\text{Bi}_2\text{Sr}_2\text{CaCu}_2\text{O}_{8+\delta}$ (2:2:1:2 structure) single crystals as well as on the effects of varying the oxygen content in unsubstituted single crystals through oxygen annealing. Attempts were also made to incorporate Na^{1+} for Ca^{2+} in the 2:2:1:2 structure, although no Na was detected in these crystals. Doped and undoped crystals have been characterized using microprobe, x-ray, thermogravimetric analysis, and magnetic and Hall measurements.

II. CRYSTAL GROWTH

The crystals used in this study were grown using a directional solidification approach employing a stationary crucible in a strong temperature gradient ($\sim 10^\circ\text{C}/\text{cm}$). As the average oven temperature decreases from above the melting point of $\text{Bi}_2\text{Sr}_2\text{CaCu}_2\text{O}_{8+\delta}$, one point or side of the crucible reaches the crystallization temperature first. A crystallization zone proceeds across the crucible as the average temperature is further reduced. The volume of the melt in this zone, at any one time, can be controlled by the size of the temperature gradient across the crucible. The growth rate of the crystals across the crucible is determined by the temperature ramp rate.

Starting materials for the crystal growth were unreacted Bi_2O_3 , SrCO_3 , CaCO_3 , and CuO for the undoped samples and, additionally, Y_2O_3 , Na_2CO_3 , and La_2O_3 for the doped crystals. All starting compounds were 99.99% purity or better, with the exception of the CaCO_3 , which was 99.95% purity. The initial starting materials were weighted out to ± 1 mg to yield an atomic ratio



Excess Bi_2O_3 ($\sim 10\%$) was included to allow for the evaporation of Bi_2O_3 during growth and to act as a flux for the crystal growth. In addition to undoped samples, crystals were grown with initial starting concentrations $y=0.05, 0.10, 0.15, 0.20, 0.30, 0.40, 0.50$, and 1.00 for Y doping, $x=0.05, 0.10, 0.25, 0.50, 1.00$, and 2.00 for La doping, and $y=0.05, 0.10, 0.15$, and 0.20 for Na doping. The unreacted and coarsely mixed starting oxides and carbonates were placed into alumina crucibles. Typically, Coors high-form alumina crucibles (CH50) were used and, approximately, 50 g of starting material was placed into each crucible. Each crucible was covered with an alumina sheet to reduce Bi evaporation and to prevent contamination from the oven during growth.

The crucibles were placed into a box oven with heating elements on three sides of the oven. In order to provide a temperature gradient, the small (relative to the internal dimensions of the oven) crucibles were pushed up against the back or side walls of the oven within, approximately, 0.5 cm from the heating elements. Chromel-alumel ther-

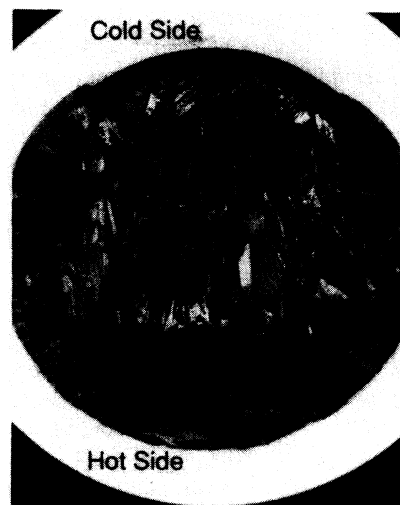


FIG. 1. Top view of an alumina crucible containing 2:2:1:2 crystals grown using a directional solidification approach. The crystals primarily nucleate on the cold side of the crucible and grow along the temperature gradient toward the hot side as the average temperature in the oven is reduced.

mocouples were placed against the hot side (heating element side) and cold side (toward oven center) of the crucibles. A temperature difference of typically 25–40°C could be maintained across the alumina crucibles (≈ 50 mm) while the crucibles were being cooled. Initially, the crucibles were heated in air to 900–930°C (all reported temperatures were measured on the cold side of the crucible), and maintained at this temperature for 2 h. The melts were then cooled in air at a rate of between 0.4–1.0°C/h to, approximately, 725°C at which point the oven was shut off and the crucibles were cooled in air to room temperature over a 3 h period.

The top view of a crucible containing undoped crystals is shown in Fig. 1. Apparent from this figure are numerous nucleation sites primarily on the cold side of the crucible and the tendency of the crystals to grow outward from these sites in an orientation with the sheets, approximately, aligned along the temperature gradient. This growth behavior is expected since the thermal conductivity in the planes of the sheets is higher than that perpendicular to the mica-like sheets.²⁰ For the crucible shown in Fig. 1, the melt does not wet the hot side of the crucible as, apparently, all of the starting material has been incorporated into the crystals before the crystal-melt interface reaches this side of the crucible. While the a - b plane preferentially grows along the temperature gradient, the rotation angle of the a - b planes with respect to an axis along the temperature gradient varies and the crystals appear to grow somewhat randomly oriented about this axis. Around the top rim of the melt, a region of greenish-yellow polycrystalline material is apparent that results from a reaction with the alumina crucible. The crucible is etched where this phase contacts it and through microprobe analysis the major constituents were found to be Bi, Al, Sr, and Ca. This polycrystalline material, however, has a sharp interface with the 2:2:1:2

crystals and Al incorporation in the crystals is, in all cases examined, quite small (<0.01 Al per formula unit).

After shattering the crucible, black, shiny, micalike crystals are removed with in-plane dimensions as large as 2 cm^2 . Perpendicular dimensions for the best single crystals, however, are only $20\text{--}100\ \mu\text{m}$. Crystals are easily removed from the melt and cleaved using a surgical scalpel. X-ray analysis confirms that the c axis of the crystals is perpendicular to the plane of the sheets.

Undoped crystals were also grown using a stoichiometric melt, $2.1\text{Bi}:1.9\text{Sr}:0.9\text{Ca}:2.1\text{Cu}$, where this composition was decided upon from a microprobe analysis (described later) of earlier grown crystals. The starting oxides and carbonates were prereacted and then melted at 1010°C . The melt was cooled at $10^\circ\text{C}/\text{h}$ to 920°C , $1^\circ\text{C}/\text{h}$ to 775°C , $30^\circ\text{C}/\text{h}$ to 300°C , and $50^\circ\text{C}/\text{h}$ to 20°C in air. As in earlier runs, the covered crucible was placed in a temperature gradient, resulting in directional growth of large (up to 2 cm^2 faces) crystals across the crucible, from cold to hot side. Only a trace of the greenish-yellow material was present around the top rim of the crucible. Sample composition and properties are similar to those grown in excess Bi_2O_3 , indicating that excess Bi_2O_3 is not crucial to the formation of large, high quality, single crystals in the $2:2:1:2$ system.

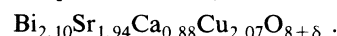
In addition to the large crystals achieved in the undoped material, large crystals were also achieved using an identical process in the lightly substituted La ($x=0.05$ and 0.10), Y ($y=0.05$), and Na ($y=0.05, 0.10$, and 0.15) melts, with the crystal size and degree of orientation in the crucible decreasing for larger dopant concentrations. Small ($1\text{--}2\text{-mm}$) single crystals were, however, achieved even when Y or La completely replaced Ca or Sr, respectively.

III. CATION STOICHIOMETRY

Wavelength-dispersive microprobe analysis [electron-probe-microanalysis technique (EPMA)], using a JEOL

superprobe 733, was performed on each batch of doped and undoped crystals to determine stoichiometry, dopant incorporation, and sample homogeneity. Standards used included Bi metal, Cu metal, SrTiO_3 , CaSiO_3 , $\text{Y}_3\text{Al}_5\text{O}_{12}$, $\text{NaAlSi}_3\text{O}_8$, and LaF_3 . An acceleration voltage of 15 kV , a beam current of 20 nA and a beam diameter of $2\text{--}10\ \mu\text{m}$ were used. Measured intensities were corrected for matrix effects using the ZAF method. Typically $3\text{--}8$ crystals from each batch were examined at five points on each crystal. Final average compositions for selected crystal growth runs with various starting compositions, both doped and undoped, are reported in Table I. The experimental uncertainty for each value in Table I is approximately ± 0.04 for each cation. For each crystal composition, only the ratio between element concentrations is important. The results for each composition are normalized to yield seven cations per formula unit.

Undoped materials yield a stoichiometry



While the ratio Bi:Cu is, approximately, 1:1, the material is apparently slightly Sr and Ca deficient relative to the expected composition $2\text{Bi}:2\text{Sr}:1\text{Ca}:2\text{Cu}$ for the ideal subcell. Sr and Ca deficiencies may be accommodated as vacancies in the crystal, substitution of Bi/Cu for Sr/Ca, or they may reflect a deviation from ideal ($2:2:1:2$) stoichiometry associated with the incommensurate periodicity observed in the structure. Sample homogeneity, on a micron scale, has been established by examining the reproducibility of the observed composition at different points on each crystal (typically five) and on ten different crystals from the same batch. The detected number of x-ray counts for each element at different points on the crystals all fall within $3\text{--}5\sigma$ of the mean value for each microprobe run, where σ is the square root of the average number of detected x-ray counts for a given element.

Introducing Y into the melt during growth was expect-

TABLE I. Melt and crystal compositions.

Substitution	Starting melt composition					Typical crystal composition						
	Bi	Sr	La	Ca	Y/Na	Cu	Bi	Sr	La	Ca	Y/Na	Cu
None	2.40	2.00		1.00		2.00	2.10	1.94		0.88		2.07
Y	2.40	2.00		0.95	0.05	2.00	2.01	1.89		0.77	0.25	2.07
	2.40	2.00		0.90	0.10	2.00	2.04	1.84		0.70	0.39	2.03
	2.40	2.00		0.85	0.15	2.00	2.00	1.82		0.59	0.49	2.12
	2.40	2.00		0.80	0.20	2.00	2.04	1.74		0.57	0.55	2.09
	2.40	2.00		0.70	0.30	2.00	2.05	1.77		0.54	0.57	2.08
	2.40	2.00		0.50	0.50	2.00	2.00	1.78		0.46	0.62	2.14
	2.40	2.00		0.00	1.00	2.00	2.06	2.15		0.00	0.71	2.08
La	2.40	1.95	0.05	1.00		2.00	2.01	1.78	0.30	0.82		2.10
	2.40	1.90	0.10	1.00		2.00	1.99	1.70	0.43	0.76		2.11
	2.40	1.75	0.25	1.00		2.00	2.03	1.57	0.51	0.82		2.07
	2.40	1.50	0.50	1.00		2.00	2.07	1.41	0.56	0.87		2.08
	2.40	1.00	1.00	1.00		2.00	2.91	1.05	1.03	0.53		1.48
	2.40	0.00	2.00	1.00		2.00	2.87	0.00	1.46	1.20		1.47
Na	2.40	2.00		0.95	0.07	2.00	2.14	1.90		0.90	0.00	2.06
	2.40	2.00		0.90	0.12	2.00	2.15	1.97		0.85	0.00	2.04
	2.40	2.00		0.80	0.23	2.00	2.19	1.98		0.79	0.00	2.04

ed to result in substitution of Y onto the Ca site since this site favors smaller ions and since Y occupies an identically coordinated site in $\text{YBa}_2\text{Cu}_3\text{O}_7$. Experimentally, substitution of Ca by Y in the melt does result in a decrease of Ca content with a corresponding increase of Y content. Single crystals of 2:2:1:2 have been formed with Ca completely replaced by Y. In addition, however, the Sr content also initially decreases with Y content, then levels off at, approximately, 1.75 Sr atoms per formula unit, and eventually rises again to 2.15, suggestive of partial Sr mixing on the Ca site for both pure Ca- and Y-doped materials. Partial Sr substitution on the oxygen depleted Ca planes is necessary for the stabilization of the $(\text{Ca}_{1-x}\text{Sr}_x)\text{CuO}_2$ system (i.e., $x=0.14$),^{21,22} apparently because of ionic size constraints in perovskite-like structures.²³ The larger atomic concentration ratio of $[\text{Sr}]:[\text{Y}]$ in the pure Y-doped crystals (despite a smaller ratio in the melt), compared with the $[\text{Sr}]:[\text{Ca}]$ ratio in the pure Ca material may reflect the need to counterbalance the smaller ionic size²⁴ of Y (1.015 Å) relative to Ca (1.12 Å).

Note that intended and actual crystal compositions may be distinctly different. For example, with an intended melt composition of



we observe a composition in the final crystals of, approximately,



For the remainder of this text specific



samples will be referred to by using the final measured crystal compositions (x,y) unless "melt composition" is explicitly noted.

Y substituted samples were less homogeneous than the undoped crystals. For all samples, the Bi and Cu atomic concentrations appear to be homogeneous, with the x-ray counts at all points examined in a given microprobe run falling within $3-5\sigma$ of the average value. However, for the Sr, Ca, and Y concentrations, the observed x-ray count rates for each element were scattered over the larger range of $\pm 10\sigma$ about the mean value, indicating a roughly 5% compositional variation for these elements over the different crystals in the crucible, and to a lesser extent across an isolated crystal. For the least substituted samples, $y=0.25$, however, substitution of Y for Ca and Sr appeared to be more homogeneous.

Besides slight compositional inhomogeneity across the different crystals, several crystals with substitution levels $y > 0.39$, investigated using backscattered electron imaging and subsequent EPMA analysis, displayed islands (typically 10–30 μm across) of distinctly different dopant concentration within the crystal. The single Cu—O layer material, $\text{Bi}_2\text{Sr}_2\text{CuO}_6$, was also occasionally observed as an inclusion in some of the most highly substituted crystals. These compositionally segregated islands typically comprise no more than a few percent of the surface ana-

lyzed. Observation of compositional segregation (rather than a continuous compositional variation between two compositions) as well as a large discrepancy between melt Y:Sr:Ca composition and final crystal composition suggests that several discrete stoichiometries (or ranges of stoichiometry) might be favored rather than a continuous homogeneity range for Y substitution. A broader series of melts is needed to resolve this question. The slight inhomogeneity on a micron scale in most samples and gross inhomogeneity in the form of islands of different composition segregating out within several of the more highly doped crystals highlight the care that must be taken when performing and especially interpreting data on cation "doped" single crystals. Homogeneity problems are expected to be even more pronounced and difficult to characterize in "doped" ceramic samples, where concentration gradients in the starting material can lead to the formation of crystallites or domains with different composition, despite a bulk sample composition identical to the starting composition.

For the La-doped samples, our intention was to replace Sr^{2+} ions on the Sr site in the 2:2:1:2 structure with La^{3+} ions, in order to compare with those samples subject to ionic replacement on the Ca site. The roughly inverse relation between La and Sr atomic concentrations is consistent with a preferential substitution of the La atoms for Sr atoms. However, mixing of the La atoms between the Sr and Ca sites cannot be ruled out by the microprobe analysis.

The 2:2:1:2 phase does not appear to be stable throughout the entire range of compositions $\text{Bi}_2(\text{Sr}_{2-x}\text{La}_x)\text{CaCu}_2\text{O}_{8+\delta}$, $0 \leq x \leq 2$, using our growth technique. Above a melt composition of, approximately, $x=0.5$ the observed stoichiometries of the single crystals examined were qualitatively different from the 2:2:1:2 composition. For both melt compositions examined with $x > 0.5$, the crystals had the stoichiometry $\text{Bi}_2(\text{Sr},\text{La},\text{Ca})_{1.8}\text{CuO}_2$, which is approximately the 2:2:0:1 composition. The sample made with melt composition $x=2.0$ formed 2:2:0:1 crystals with Sr completely replaced by La and Ca.

Homogeneity for the La-substituted samples appears to be similar to the Y-doped samples. Bi concentration appears homogeneous, while La, Sr, Ca, and additionally Cu data show evidence for slight inhomogeneity. No segregation into macroscopic islands of distinct composition were observed (using backscattered electrons) in the La-substituted samples, although the possibility of this happening in some sample cannot be ruled out.

Finally, no evidence of Na incorporation is found in crystals grown from melts with Ca partially replaced by Na. However, as the Ca concentration in the melt decreases, the final Ca content in the crystal decreases, while the Sr and Bi contents increase to compensate (Table I). Partial mixing or substitution of Bi, Sr, and Ca on their ideal sites must be present to allow for this range of compositions. Attempts were also made to jointly incorporate Na^{1+} for Ca^{2+} and La^{3+} for Sr^{2+} to satisfy charge neutrality without introducing extra oxygen or changing the oxidation states of the Cu or Bi ions. Again, no Na was detected in the crystals.

IV. OXYGEN STOICHIOMETRY

Besides ionic substitutions, the possibility of altering the oxygen stoichiometry was also explored. Based on preliminary thermogravimetric analysis (TGA) and differential thermal analysis (DTA) studies on the 2:2:1:2 and related compounds, the following annealing schedules were decided upon. Several crystals were annealed in flowing oxygen at 840°C for 6 h, slow cooled at 60°C/h to 600°C and then oven cooled to below 200°C. Additionally, some of these crystals were oxygen annealed at 5 atm and then 12 atm at 540°C for 18 h and quickly (1 h) cooled to room temperature. Finally, several of the oxygen-annealed crystals were later argon annealed at 725°C for 10 h. At each stage of the annealing sequence, crystals were removed for analysis. The composition of several crystals, before and after oxygen annealing, were determined using microprobe analysis and no change in cation stoichiometry was detected.

Thermogravimetric analysis using a Dupont 951 TGA system, was used to determine changes in oxygen contents during annealing. The balance resolution is 2 μ g and the typical starting sample was a collection of crystals weighing, approximately, 100 mg. Uncertainties in starting sample cation composition result in relatively large uncertainties on the absolute value of δ (approximately ± 0.1). However, the differences in the oxygen contents between oxygen annealed and unannealed crystals, coming from the same crystal growth runs, have a significantly smaller uncertainty.

A typical TGA analysis is shown in Fig. 2. The sample is initially heated in flowing 15% H_2 -85% He to 150°C and held for several hours to remove adsorbed gases and moisture from the sample and sample pan. In a typical run, a fairly large weight loss (0.5–1.0%) occurs during this initial phase as seen in Fig. 2. This weight loss was shown to be due to adsorbed gases or water by comparing a TGA run for a sample that was annealed in a tube furnace, removed to laboratory air for several days and then reduced in the TGA, to one that was annealed in the TGA and measured immediately without removing the

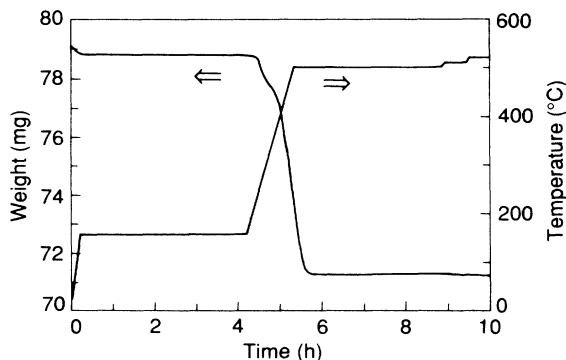


FIG. 2. Thermogravimetric analysis of a 12 atm oxygen-annealed crystal in 15% H_2 /85% He . The weight loss corresponds to the complete reduction of the sample to Bi, Cu, and (Sr,Ca)O. Note that the initial weight loss during the 150°C bake out corresponds to adsorbed gases and water.

sample from the TGA. Only the sample that sat in air for several days demonstrated the large initial weight loss at low temperatures.

After the initial bake out at 150°C, the temperature is ramped to 500°C and held for several hours in order to destructively reduce the $Bi_2Sr_2CaCu_2O_{8+\delta}$ sample (in a 15% H_2 -85% He atmosphere) to $2Bi + (2Sr,Ca)O + 2Cu$. The measured weight loss yields δ . Weight loss begins as early as 175°C in the 2:2:1:2 crystals, indicating that some of the oxygen is loosely bound in this structure. To ensure that the reduction reaction is complete by 500°C, the temperature is ramped to 520°C in two steps and the sample weight monitored to detect any further significant weight loss. Care must be taken not to raise the temperature much above this or a weight loss due to Bi evaporation will occur.

Annealing an unannealed, unsubstituted sample in 1-atm oxygen results in the uptake of 0.23(5) oxygens per formula unit, while the additional oxygen uptake observed when considering a 12-atm O_2 annealed sample is only 0.06(5) oxygens. The largest change in oxygen content is therefore seen to be in going between the unannealed and 1-atm O_2 annealed samples.

La and Y samples were also measured and the results demonstrate that substitution of trivalent Y or La ions for divalent Ca or Sr ions is accompanied by at least enough oxygen uptake to counterbalance the valence difference. The La-doped $x=0.30$ and 0.43 samples each yielded an oxygen content 0.4(1) above that of the unannealed unsubstituted samples. The Y-doped $y=0.25$ sample also demonstrates an oxygen content enhancement with an oxygen content of +0.3(1) relative to the oxygen content of the unannealed, unsubstituted samples. TGA measurements on both the ion-substituted and oxygen-annealed samples demonstrate that the 2:2:1:2 system can accommodate a significant variation in oxygen contents and therefore that oxygen content is an important parameter when considering doping in the 2:2:1:2 structure.

V. X-RAY ANALYSIS

X-ray diffraction data were collected along the a , b , and c crystallographic axes, using a four-circle diffractometer, to examine the lattice constants, incommensurate superstructure period, degree of twinning, and phase homogeneity for several of the ion- and oxygen-doped crystals (Table II). The $K\alpha$ radiation from a rotating copper anode was selected with a vertically focusing graphite monochromator before the sample. A flat graphite monochromator was placed after the sample. The maximum scattering angle used in this study was $2\theta=80^\circ$. Typical sample dimensions were $2 \times 2 \times 0.03$ mm^3 .

The subcells for samples without ion substitutions display tetragonal symmetry within the experimental resolution. However, the incommensurate superstructure, along one of the axes (b_0) breaks the symmetry between the a and b axes. We note that no twinning is observed in samples without ion substitutions. Both of the Y-doped samples are highly twinned and exhibit weak

TABLE II. Lattice parameters for ion- and oxygen-doped samples.

Doping	Sample	Lattice constants (\AA)			Superstructure period ($x b_0$)	
		a_0	b_0	c_0		
Oxygen-annealed 2:2:1:2	no anneal (crystal 1)	5.413(2)	5.411(3)	30.91(1)	4.7(1)	
	no anneal (crystal 2)	5.413(2)	5.411(2)	30.89(1)	4.8(1)	
	1-atm O_2	5.411(2)	5.414(2)	30.80(1)	4.7(1)	
	5-atm O_2	5.409(2)	5.414(2)	30.81(1)	4.8(1)	
	12-atm O_2	5.408(2)	5.413(2)	30.81(1)	4.7(1)	
Ion-substituted 2:2:1:2	Y	$Bi_{2.01}Sr_{1.89}Ca_{0.77}$ $Y_{0.25}Cu_{2.07}O_{8+\delta}$	5.406(4)	5.409(4)	30.83(1)	4.6(1)
		$Bi_{2.06}Sr_{2.15}Y_{0.71}$ $Cu_{2.08}O_{8+\delta}$	5.432(2)	5.467(2)	30.23(1)	4.1(1)
	La	$Bi_{2.01}Sr_{1.78}La_{0.30}$ $Ca_{0.82}Cu_{2.10}O_{8+\delta}$	5.416(2)	5.425(2)	30.71(1)	4.6(1)
		$Bi_{1.99}Sr_{1.70}La_{0.43}$ $Ca_{0.76}Cu_{2.11}O_{8+\delta}$	5.435(2)	5.440(2)	30.55(1)	4.7(1)

reflections for the single layer 2:2:0:1 material, consistent with the microprobe-scanning-electron-microscopy (SEM) analysis that detected islands of single layer material intergrown in the more highly substituted of these samples. The La-doped crystals are not twinned, but examination of the shape of several reflections in a 2θ scan for the more highly doped crystal yield evidence for compositional segregation as a second set of diffraction lines appear, which are very close to the main lines but distinguishable. For both the La- and Y-substituted samples, x-ray diffraction confirms the presence of phase and/or compositional segregation within a crystal, as discussed earlier in the microprobe analysis section. These problems are however, significantly reduced in the least substituted La- and Y-doped samples.

Oxygen annealing produces very little change in the a_0 and b_0 lattice parameters or in the incommensurate superstructure period that remains at, approximately, $4.7b_0$ for each of the samples. However, a very distinct difference is seen in the c -axis dimension between the unannealed samples (30.90 \AA) and all of the oxygen-annealed samples (30.81 \AA). This apparent step in the c -axis parameter with oxygen annealing most likely reflects the large difference in oxygen content between unannealed and 1-atm oxygen-annealed samples versus the much smaller difference between the 1- and 12-atm oxygen-annealed samples. However, a subtle structural change, perhaps occurring in the BiO planes, where oxygen content variation is apparently accommodated,²⁵ cannot be ruled out.

Replacing Sr with La results in a significant decrease of the c_0 lattice parameter to 30.55 \AA for $x=0.43$, while the a_0 and b_0 parameters increase to $a_0=5.435(2) \text{ \AA}$ and $b_0=5.440(2) \text{ \AA}$. Similar behavior is observed in the Y-substituted sample, where the c_0 parameter decreases to 30.23 \AA and the a_0 and b_0 parameters increase to $a_0=5.432(2) \text{ \AA}$ and $b_0=5.467(2) \text{ \AA}$ for $y=0.71$ and no Ca. The superstructure period appears to be relatively insensitive to ion substitutions for small substitution levels, but for $y=0.71$ it has been reduced to $4.1b_0$.

VI. MAGNETIC MEASUREMENTS

Magnetic measurements were obtained using a Quantum Design (SQUID) magnetometer. Superconducting properties were typically studied by cooling the sample in the magnet remanent field ($\sim 1 \text{ Oe}$) and measuring the sample magnetization as it is warmed up in this field.

Figure 3 shows the effect of oxygen annealing on the Meissner transition in a single crystal with no La or Y substitution. These data are all taken on the same crystal, with the field applied parallel to the c axis, after each anneal at progressively higher oxygen pressures and finally in argon. Annealing an as grown crystal in flowing oxygen with a slow cool (as described before) reproducibly yields a reduction of T_c^{onset} from 90 to 84 K, while the

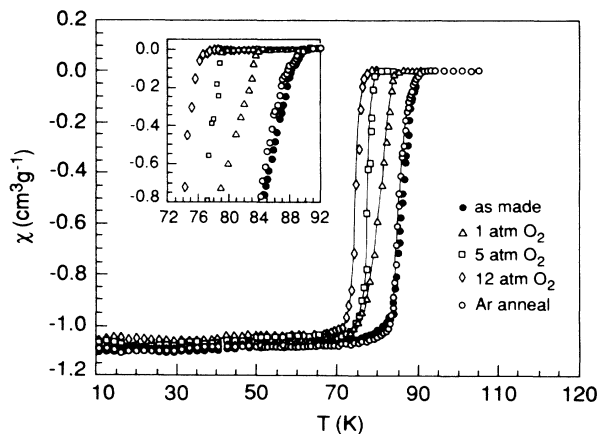


FIG. 3. Field-cooled superconducting transitions taken using a field ($\approx 1 \text{ Oe}$) applied parallel to the c axis of a single 2:2:1:2 crystal with no ion substitutions. The same crystal was progressively annealed at higher oxygen pressures and finally in argon, demonstrating a reversible progression between a 77 and 90 K superconductor.

magnitude of the Meissner transition and the sharpness of the superconducting transition remain *virtually identical*. Further suppression of T_c^{onset} from 84 to 79 K and finally to 77 K is observed after the 5- and 12-atm oxygen pressure anneals, respectively. Reversibility was demonstrated by annealing at 725°C in argon, after which the 90 K transition was completely recovered. Transition widths (10–90% of complete transition) of 2–5 K are observed and *no* transition width broadening or change in low-temperature Meissner signal is observed as the transition temperature is reduced from 90 to 77 K. Samples were also examined with the *ab* planes aligned parallel to the magnetic field so that the demagnetization factor, $1/1-n$, is, approximately, 1. In this geometry, the observed flux expulsion is approximately 80% of complete diamagnetism.

Figures 4(a) and 4(b) show the magnetic onsets of superconductivity for several of the Y- and La-doped samples, respectively. In each case, all measurements are made in the same remanent field (≈ 1 Oe) and each sample is oriented with the crystallographic *c* axis parallel to the applied field. For the lower La-substitution levels—i.e., $x=0.30$ and 0.43 —the superconducting transition temperatures and transition widths are relatively insensitive to whether the system is “doped,” despite rather large levels of substitution. The Y-substituted $y=0.25$ sample also has only a slightly higher onset temperature (≈ 92 K) than for the undoped samples. The general insensitivity of T_c and Meissner signal to the smaller ion-substitution levels is likely due to the oxygen pulled into the structure to compensate the replacement of divalent

by trivalent ions. For larger Y- or La-substitution levels, however, the transition widths rapidly broaden and the Meissner signal decreases precipitously, while the onset temperature only decreases marginally. The broadening of the superconducting transition and disappearance of the Meissner signal most likely can be attributed to phase segregation and inhomogeneity as observed in these samples using microprobe and x-ray diffraction analyses.

Normal-state magnetic properties were looked at for temperatures above the superconducting transition temperature using a 50 kOe field applied parallel to the *c* axis of each crystal. The magnetic response from the sample holder was measured separately and subtracted.

Figure 5 demonstrates the effect of increased oxygen content on the normal-state magnetization of samples with no ion substitutions. The susceptibility is enhanced with oxygen annealing and can be returned to the as made value by annealing in argon. Pauli susceptibilities are extracted from the displayed data by assuming that the measured susceptibility can be expressed as a sum,

$$\chi = \chi_{\text{Pauli}} + \chi_{\text{Landau}} + \chi_{\text{core}} + \chi_{\text{Curie}}(1/T).$$

The roughly temperature-independent behavior (or even χ increasing with T behavior in the as made samples) above T_c , allows us to neglect the χ_{Curie} term. Core diamagnetism can be calculated using tabulated values²⁶ for the ions present and is, approximately, $\chi_{\text{core}} = -2.30 \times 10^{-7} \text{ cm}^3/\text{g}$ for the samples without ion substitution. For a gas of free fermions with effective mass m^* ,

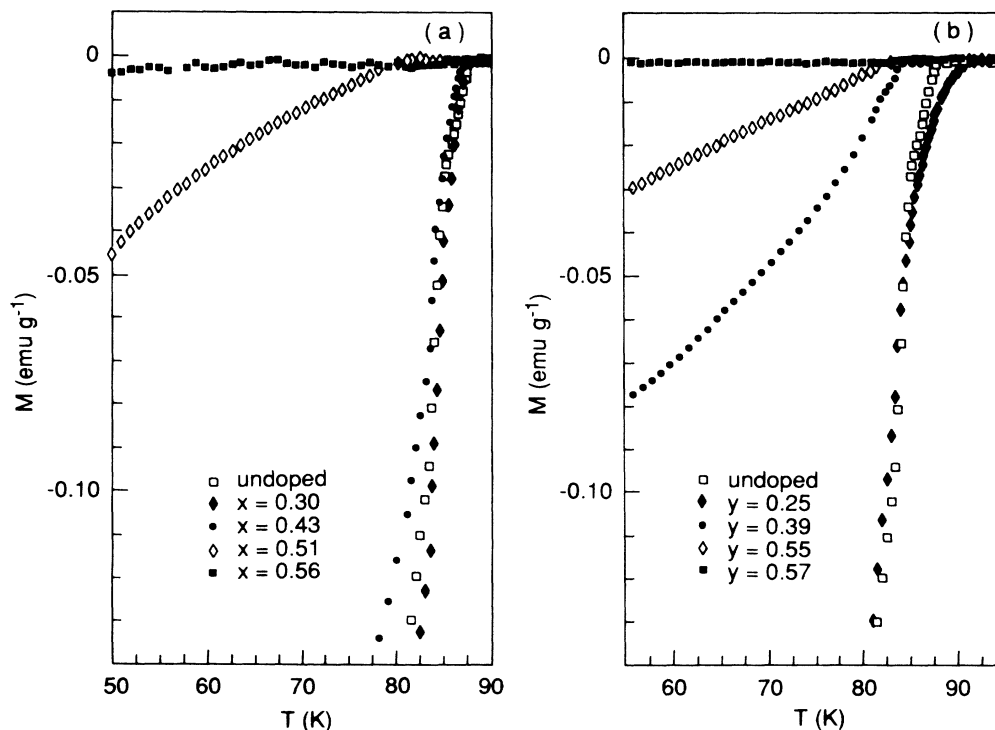


FIG. 4. Field-cooled superconducting transitions taken using a 1 Oe field applied parallel to the *c* axis for (a) La-substituted and (b) Y-substituted samples. The compositions x, y refer to the actual La and Y contents, respectively.

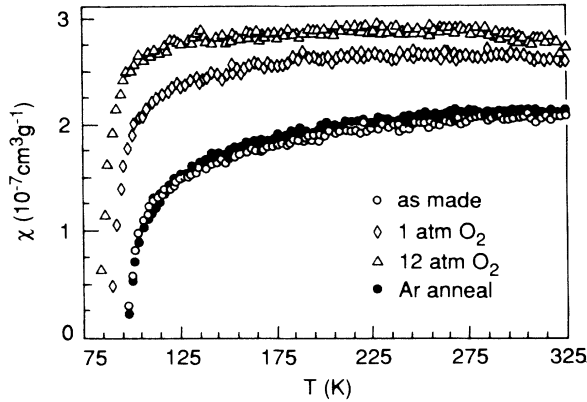


FIG. 5. Normal-state magnetic-susceptibility data for the oxygen annealed 2:2:1:2 crystals as a function of temperature and annealing conditions. The 50-kOe field was applied parallel to the crystallographic c axis.

$$\chi_{\text{Landau}} = -\frac{1}{3}(m_e/m^*)^2 \chi_{\text{Pauli}},$$

where m_e is the free electron mass. In light of the enhanced effective masses typically observed in the cuprate superconductors, χ_{Landau} is expected to be at least 1 order of magnitude smaller than χ_{Pauli} and will be neglected in this analysis. The values for χ_{Pauli} computed using the values for χ at 270 K are listed in Table III along with the corresponding density of states $g(\epsilon_f)$ obtained using the relation, $\chi_{\text{Pauli}} = \mu_b^2 g(\epsilon_f)$.

The density of states $g(\epsilon_f)$ varies from 6.1 states per eV Cu site for the unannealed samples to 7.2 states per eV Cu site for the 12-atm O_2 annealed samples. These values are, approximately, a factor of 2 higher than predicted by band-structure calculations.²⁷ Elevated magnetic susceptibility obtained density of states values, compared with band-structure calculations, have also been observed in other cuprate superconductors.⁵

Normal-state magnetization data for the lightly ion-doped single crystals are shown in Fig. 6 and the computed Pauli susceptibilities are listed in Table III. The La-doped sample with $x=0.30$ has virtually the same T_c as the undoped, unannealed single crystals and also has, approximately, the same normal-state susceptibility. It is

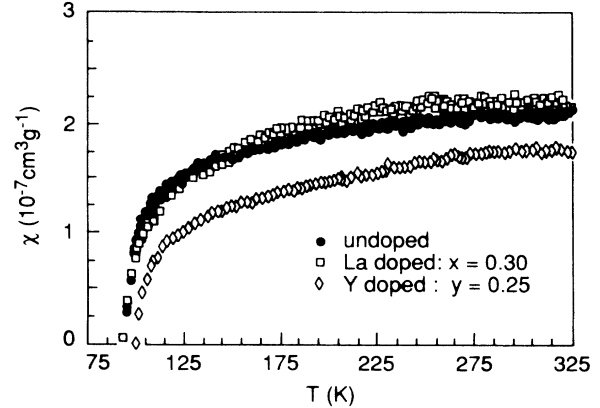


FIG. 6. Comparison of the normal-state magnetic susceptibility for unsubstituted and lightly Y and La substituted 2:2:1:2 crystals. The 50-kOe field was applied parallel to the crystallographic c axis.

important to note, however, that the $x=0.30$ sample has significantly different lattice constants than the unannealed, unsubstituted sample (Table II), thereby suggesting that T_c is not as strongly coupled to the structural changes as it is to the density of states in this doping regime. The Y-doped sample with Y content $y=0.25$ has a slightly higher T_c^{onset} and slightly lower density of states, consistent with the oxygen-doped samples that display an inverse relation between $g(\epsilon_f)$ and T_c in the range of doping considered.

VII. HALL EFFECT

Hall measurements were performed on the as made, 1- and 12-atm oxygen-annealed crystals to determine if the increasing oxygen contents in these samples contribute extra mobile carriers. Note that in the $\text{YBa}_2\text{Cu}_3\text{O}_{7-x}$ system, this is not true over the entire range $0 \leq x \leq 1$, since some holes become localized on the oxygen deficient Cu—O chain layer.²⁸ It is of interest to see if there is a similar charge reservoir in the 2:2:1:2 system.

The crystals were examined in cross section under an optical microscope to insure thickness uniformity. For average thickness determination, however, the crystals

TABLE III. Normal-state susceptibility for superconducting ion- and oxygen-doped samples.

Doping	Sample	χ_{Pauli} (10^{-7} cm ³ /g)	$g(\epsilon_f)$ (states per eV Cu site)
Oxygen-annealed 2:2:1:2	no anneal	4.3	6.1
	1 atm	4.9	6.9
	5 atm	5.0	7.0
	12 atm	5.2	7.2
	Ar anneal	4.4	6.1
Ion-substituted 2:2:1:2	Y	$\text{Bi}_{2.01}\text{Sr}_{1.89}\text{Ca}_{0.77}$ $\text{Y}_{0.25}\text{Cu}_{2.07}\text{O}_{8+\delta}$	5.6
	La	$\text{Bi}_{2.01}\text{Sr}_{1.78}\text{La}_{0.30}$	6.3
		$\text{Ca}_{0.82}\text{Cu}_{2.10}\text{O}_{8+\delta}$	4.5

were weighed and the thicknesses calculated using the measured in-plane dimensions and the known density. Thicknesses ranged from 10–50 μm . Silver paint contacts were used in a standard five point contact geometry. The 5.5-T magnetic field was applied parallel to the 2:2:1:2 crystallographic c axis. A dc current of 10 A/cm² was used although several other applied fields and currents were also used to check the linearity of the Hall voltage with respect to both current and magnetic field. Three different crystals were examined for each oxygen treatment, using both polarities of current and field, thereby yielding an average value for the Hall voltage for each group of samples. A platinum thermometer was used to determine the sample temperature in zero applied magnetic field.

Figure 7 shows the temperature dependence of the Hall constant R_H for the unannealed and 12-atm oxygen-annealed samples. Hall measurements on the $\text{YBa}_2\text{Cu}_3\text{O}_{7-x}$ (with x close to zero) system yield data with pronounced temperature dependence,^{29,30} complicating the interpretation of the Hall carrier concentration, at least within a single band model. The Hall effect in the 2:2:1:2 single crystals appears to demonstrate a less pronounced temperature dependence with R_H (100 K)/ R_H (270 K) \approx 1.3 as opposed to R_H (100 K)/ R_H (270 K) \approx 3.0 for the $\text{YBa}_2\text{Cu}_3\text{O}_7$ system.

The measured Hall carrier density for the unannealed samples at 270 K, $3.1(3) \times 10^{21} \text{ cm}^{-3}$ (0.34 holes per Cu site), is consistent with values in the literature for unannealed, unsubstituted 2:2:1:2 single crystal samples,³¹ especially given the likelihood of small stoichiometry differences between the samples. Annealing in 1 atm of oxygen increases the carrier density to $3.7(2) \times 10^{21} \text{ cm}^{-3}$ (0.40 holes per Cu site), while further annealing in 12-atm oxygen results in $4.6(3) \times 10^{21} \text{ cm}^{-3}$ (0.50 holes per Cu site).

The carrier concentrations for the unannealed and oxygen-annealed 2:2:1:2 single crystals can be compared

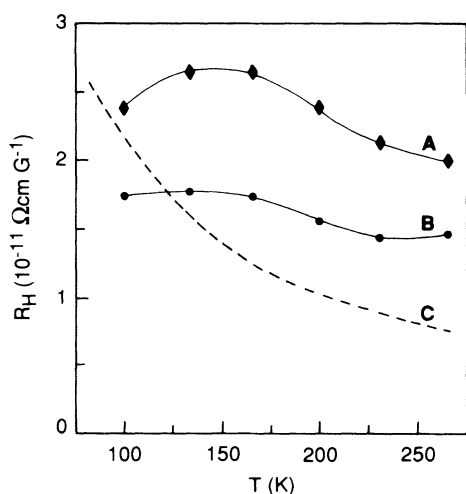


FIG. 7. Hall resistance, R_H vs temperature for A: an unannealed 2:2:1:2 crystal; B: a 12-atm oxygen-annealed 2:2:1:2 crystal; and C: a $\text{YBa}_2\text{Cu}_3\text{O}_7$ thin film (data from Ref. 29).

with the values obtained for the $T_c = 90$ K $\text{YBa}_2\text{Cu}_3\text{O}_7$ phase,^{28,30} approximately, 0.25 holes per Cu{2} site (in the Cu—O planes), and the $T_c \approx 60$ K $\text{YBa}_2\text{Cu}_3\text{O}_{6.6}$ phase,³⁰ approximately 0.12 holes per Cu{2} site. While the unannealed sample has a concentration only slightly larger than that found in $\text{YBa}_2\text{Cu}_3\text{O}_7$, the values for the oxygen annealed samples diverge further from this value.

The fact that T_c decreases with increasing oxygen content and carrier concentration in the 2:2:1:2 crystals can be rationalized in terms of the relatively large carrier concentrations, starting at 0.34 holes per Cu site for the unannealed samples and increasing to 0.50 holes per Cu site in the 12-atm O_2 annealed samples. Data for cation-doped $\text{Bi}_2(\text{Sr,Ca})_3\text{Cu}_2\text{O}_{8+\delta}$ (Refs. 32 and 33) $\text{YBa}_2\text{Cu}_3\text{O}_{7-x}$, and $\text{La}_2\text{CuO}_{4-y}$ (Ref. 28) ceramics suggest a maximum in T_c versus mobile hole concentration on the Cu—O sheets (i.e., neglect the localized holes in the Cu—O chain layer of $\text{YBa}_2\text{Cu}_3\text{O}_{7-x}$) at around 0.2–0.3 holes per Cu site. Since we are in a regime above this maximum, the decrease in T_c with n is consistent with earlier studies on cation-substituted ceramics. It is important to note, however, that all prior doping studies that probed the high-carrier-concentration regime, of which we are aware, suffered from degradation of the superconducting properties above the optimal (i.e., yielding the highest T_c in the material) doping concentration. Broadened transitions and depressed low-temperature Meissner signals call into question the microscopic homogeneity of these samples and consequently the intrinsic nature of the decrease in T_c above $n \approx 0.3$ carriers per Cu site. The observed decrease in T_c with carrier concentration in this study with $0.3 \leq n \leq 0.5$ holes per Cu site, without degradation of the superconducting properties or any other evidence of inhomogeneity or phase segregation, confirms that this maxima in T_c versus n is an intrinsic property of the double Cu—O layer high-temperature superconductors.

We can also compare the change in carrier concentration with the change in oxygen content. In going from the unannealed to the 12-atm oxygen-annealed samples, the carrier concentration increases by 0.32(3) holes per formula unit, while the oxygen content increases by, approximately, 0.29(5) oxygens per formula unit contributing an extra 0.58 holes per formula unit. The discrepancy between the number of holes theoretically contributed by the extra oxygen and the number of mobile holes actually measured in the Hall measurements suggests that some of the added holes do not contribute to the mobile carrier concentration as is the case in $\text{YBa}_2\text{Cu}_3\text{O}_{7-x}$, $0 \leq x \leq 1$. In the case of $\text{YBa}_2\text{Cu}_3\text{O}_{7-x}$ these extra holes get localized on the oxygen-deficient Cu—O chain layer, whereas for the 2:2:1:2 system, it is likely these holes partially oxidize the Bi—O layer.

Finally, using the measured density of states from the magnetic-susceptibility data and the carrier concentrations described here, the relation between the two is found to be consistent with the anisotropic three-dimensional Fermi gas relation, $g(\epsilon_f) \propto m^* n^{1/3}$, with

$$m^* = m_{xy}^{2/3} m_z^{1/3} = 9.2(3) .$$

We note, however, that more precise data over a considerably wider range of carrier concentrations is necessary to establish whether this system actually obeys a 3D Fermi liquidlike relation, over an appreciable range of carrier concentration.

VIII. CONCLUSION

A directional solidification method has been described for the growth and preparation of ion-doped (La for Sr and Y for Ca) and oxygen-doped single crystals in the $\text{Bi}_2\text{Sr}_2\text{CaCu}_2\text{O}_{8+\delta}$ system. The critical aspect of this growth technique is the use of a temperature gradient to limit the region of the crucible in which the nucleation takes place and to orient the growth of the crystals. Thin (10–100 μm) mica-like single crystals have been grown using this technique with in-plane dimensions as large as 2 cm^2 .

Oxygen annealing a 2:2:1:2 single crystal in increasing partial pressures of oxygen results in a reduction of T_c from 90 to 77 K. Most significantly, however, this change in T_c with doping is not accompanied by a broadening of the superconducting transition nor a reduction in low-temperature Meissner signal, as is typically seen in oxygen- or ion-doped $\text{YBa}_2\text{Cu}_3\text{O}_{7-x}$ or $\text{La}_2\text{CuO}_{4-y}$. The doping-induced degradation effects in these compounds, as well as in the more highly ion substituted 2:2:1:2 crystals, can be explained in terms of inhomogeneity on a microscopic scale and phase segregation as the system is pushed away from an ordered state or preferred composition and in terms of the very small coherence length in these materials. The closest analogy to the oxygen doping in the 2:2:1:2 system is the existence of two distinct superconducting compositions in the $\text{YBa}_2\text{Cu}_3\text{O}_{7-x}$ system as a function of oxygen content, the $T_c=90$ K ($x=0$) and the 60 K ($x\approx 0.4$) compositions.⁵⁰ The apparently monotonic variation of the superconducting transition temperature (with narrow transition widths), carrier concentration, oxygen content, and normal-state magnetization with oxygen annealing strongly suggests that this system can be tuned at least approximately continuously. This system therefore appears to be ideal for pursuing the very important questions relating to how properties change with carrier concentration.

The Hall-effect carrier concentration observed in the unannealed and oxygen-annealed samples range from 0.34 mobile holes per Cu site (unannealed, $T_c=90$ K) to 0.50 mobile holes per Cu site (12-atm O_2 , $T_c=77$ K). These values are high compared to the value obtained in the $T_c=90$ K $\text{YBa}_2\text{Cu}_3\text{O}_7$ material, where $n\approx 0.25$ mobile holes per Cu{2} site.^{28,30} The reduction of T_c with n in this high-carrier-concentration regime, without evidence for inhomogeneity or phase segregation with increased doping, confirms findings on ceramics that there is a high carrier concentration regime in which T_c decreases with n (i.e., this cannot be ascribed to materials problems).

Ion substitutions provide an interesting extra degree of freedom in the study of doping in the 2:2:1:2 system. For both Y- and La-substituted samples, x-ray diffraction and

microprobe analysis indicate problems with inhomogeneity and phase segregation in the more highly substituted samples. These material problems manifest themselves in the superconducting properties as broadened transitions and a reduced low-temperature Meissner signal. However, for the lower substitution levels (<20–25%), homogeneity appears to be less of a problem. Small quantities ($x\approx 0.3$) of La substituted for Sr results in little or no change in T_c or density of states $g(\epsilon_f)$, as measured using magnetic susceptibility, when compared with an unsubstituted sample prepared similarly. This results from the extra oxygen taken into these samples which counteracts the trivalent for divalent substitution. However, while T_c and $g(\epsilon_f)$ do not change, the structure does change. For the unannealed, unsubstituted sample $a_0=5.413(2)$, $b_0=5.411(2)$, and $c_0=30.90(1)$, with an incommensurate superstructure period of $4.8(1)b_0$, while for the



sample, $a_0=5.416(2)$, $b_0=5.425(2)$, $c_0=30.71(1)$ and the incommensurate superstructure period is $4.6(1)b_0$. Combined with the observation that for the oxygen-annealed samples, the structure remains unchanged within experimental resolution, while T_c shifts with $g(\epsilon_f)$, it is shown that the sensitivity of T_c to doping in this doping regime derives from the changes in carrier concentration or density of states, rather than from variations in structural parameters induced by the doping.

In all of the samples considered in this paper, variation in oxygen content plays an important role in determining sample properties. A reasonable guess is that this oxygen is principally incorporating into the Bi—O layers since these layers are strained as they try to stretch over the Cu—O layers. The incommensurate periodicity observed in the 2:2:1:2 material appears to be due to a periodic modulation of the Bi—O bond lengths³⁴ in the Bi—O planes. The oxygen bound to the Bi with the longest bonds is expected to be loosely bound and may be at least partially responsible for the oxygen stoichiometry variation upon annealing.

In going from the unannealed to the 12-atm O_2 annealed sample, the change in sample oxygen content is approximately 0.29(5) oxygens per formula unit. Comparing this with the actual change in effective mobile carrier concentration, $\Delta n=0.32(3)$ holes per formula unit, we find that approximately half of the holes contributed by the additional oxygen contribute to the mobile carrier concentration. The rest are likely to be associated with the Bi—O plane, where they can effectively oxidize Bi^{3+} to Bi^{5+} . The Bi—O layer in the 2:2:1:2 plays a similar role as the Cu—O chain layer in the $\text{YBa}_2\text{Cu}_3\text{O}_7$ material in that it is capable of acting as a charge reservoir. The existence of an electrically (and mechanically) “soft” layer that can act as a charge reservoir appears to be a common feature among the double Cu—O layer superconductors.

Another interesting factor to consider in a doping study includes the dependence of the density of states at ϵ_f on the density of carriers n . While our data is consistent with $m^*n^{1/3}$ behavior, with an effective mass of

$m^* = 9.2(3)m_e$, a considerably wider range of carrier concentration and tighter error bars in the carrier concentration data are necessary to establish the exponent carefully enough to decide that the density of states obeys a Fermi-liquid-type relation over an appreciable range of carrier concentration. A wider range of carrier concentrations and T_c 's may be possible by higher pressures of oxygen during annealing and hydrogen anneals at low temperature ($< 250^\circ\text{C}$).

Taken together, the data demonstrates that reversible and reproducible continuous changes in superconducting and normal-state properties can be made to occur in homogeneous single crystals of "2212" by oxygen doping. Simple models for the transport and magnetic data have been used to highlight the appearance of nontrivial corre-

lations among them. More complete treatments will be presented elsewhere.

ACKNOWLEDGMENTS

Two of the authors would like to acknowledge support received from AT&T (D.B.M.) and the National Science Foundation (A.K.). We would also like to thank Professor W. Harrison and Julie Paque for helpful discussions and Mark Lee for help with the Hall measurements. This work was supported in part by the Joint Services Electronic Program under Grant No. N00014-84-K-0327 and by the Stanford Center for Materials Research through the National Science Foundation Department of Materials Research.

- ¹D. B. Mitzi, J. Z. Sun, D. J. Webb, M. R. Beasley, T. H. Geballe, and A. Kapitulnik (unpublished).
- ²S. A. Sunshine, L. F. Schneemeyer, J. V. Waszczak, D. W. Murphy, S. Miraglia, A. Santoro, and F. Beech, *J. Cryst. Growth* **85**, 632 (1987).
- ³E. M. McCarron III, C. C. Torardi, J. P. Attfield, K. J. Morrissey, A. W. Sleight, D. E. Cox, R. K. Bordia, W. E. Farneth, R. B. Flippen, M. A. Subramanian, E. Lopdrup, and S. J. Poon, in *High-Temperature Superconductors*, Proceedings of the Materials Research Society, Anaheim, 1987, edited by M. B. Brodsky, R. C. Dynes, K. Kitazawa, and H. C. Tuller (Materials Research Society, Pittsburgh, 1987), p. 19.
- ⁴C. U. Segre, B. Dabrowski, D. G. Hinks, K. Zhang, J. D. Jorgensen, M. A. Beno, and I. K. Schuller, *Nature (London)* **329**, 227 (1987).
- ⁵D. B. Mitzi, P. T. Feffer, J. M. Newsam, D. J. Webb, P. Klavins, A. J. Jacobson, and A. Kapitulnik, *Phys. Rev. B* **38**, 6667 (1988).
- ⁶J. M. Tarascon, L. H. Greene, W. R. McKinnon, G. W. Hull, and T. H. Geballe, *Science* **235**, 1373 (1987).
- ⁷M. W. Shafer, T. Penney, and B. L. Olson, *Phys. Rev. B* **36**, 4047 (1987).
- ⁸R. Yoshizaki, Y. Saito, Y. Abe, and H. Ikeda, *Physica* **152C**, 408 (1988).
- ⁹Y. Ando, K. Fukuda, S. Kondoh, M. Sera, M. Onoda, and M. Sato, *Solid State Commun.* **67**, 815 (1988).
- ¹⁰N. Fukushima, H. Niu, and K. Ando, *Jpn. J. Appl. Phys.* **27**, L790 (1988).
- ¹¹A. K. Ganguli, R. Nagarajan, K. S. Nanjundaswamy, and C. N. R. Rao, *Mater. Res. Bull.* **24**, 103 (1989).
- ¹²N. Fukushima, H. Niu, and K. Ando, *Jpn. J. Appl. Phys.* **27**, L1432 (1988).
- ¹³T. Tamegai, A. Watanabe, K. Koga, I. Oguro, and Y. Iye, *Jpn. J. Appl. Phys.* **27**, L1074 (1988).
- ¹⁴N. Nishida, H. Miyatake, S. Okuma, T. Tamegai, Y. Iye, R. Yoshizaki, K. Nishiyama, and K. Nagamine, *Physica* **156C**, 625 (1988).
- ¹⁵T. Oashi, K. Kumagai, Y. Nakajima, T. Tomita, and T. Fujita, *Physica* **157C**, 315 (1989).
- ¹⁶A. Manthiram and J. B. Goodenough, *Appl. Phys. Lett.* **53**, 420 (1988).
- ¹⁷J. M. Tarascon, P. Barboux, G. W. Hull, R. Ramesh, L. H. Greene, M. Giroud, M. S. Hegde, and W. R. McKinnon, *Phys. Rev. B* **39**, 4316 (1989).
- ¹⁸H. W. Zandbergen, W. A. Groen, G. van Tendeloo, and S. Amelinckx, *Appl. Phys. A* (to be published).
- ¹⁹D. R. Harshman, G. Aeppli, B. Batlogg, G. P. Espinosa, R. J. Cava, A. S. Cooper, L. W. Rupp, E. J. Ansaldo, and D. L. Williams, *Phys. Rev. Lett.* **63**, 1187 (1989).
- ²⁰J. T. Fanton, D. B. Mitzi, A. Kapitulnik, B. T. Khuri-Yakub, G. S. Kino, D. Gazit, and R. S. Feigelson, *Appl. Phys. Lett.* **55**, 598 (1989).
- ²¹R. S. Roth (unpublished).
- ²²T. Siegrist, S. M. Zahurak, D. W. Murphy, and R. S. Roth, *Nature (London)* **334**, 231 (1988).
- ²³K. K. Singh, P. Ganguly, and J. B. Goodenough, *J. Solid State Chem.* **52**, 254 (1984).
- ²⁴R. D. Shannon and C. T. Prewitt, *Acta Crystallogr. Sect. B* **26**, 925 (1969).
- ²⁵H. W. Zandbergen, W. A. Groen, F. C. Mijlhoff, G. van Tendeloo, and S. Amelinckx, *Physica* **156C**, 325 (1988).
- ²⁶*Landolf-Berstein* (new series), edited by K.-H. Hellwege and A. M. Hellwege (Springer-Verlag, Heidelberg, 1986), Vol. II/16, p. 402.
- ²⁷F. Herman, R. V. Kasowski, and W. Y. Hsu, *Phys. Rev. B* **38**, 204 (1988).
- ²⁸M. W. Shafer, J. Penney, B. L. Olson, R. L. Greene, and R. H. Kochi, *Phys. Rev. B* **39**, 2914 (1989).
- ²⁹K. Char, Mark Lee, R. W. Barton, A. F. Marshall, I. Bozovic, R. H. Hammond, M. R. Beasley, T. H. Geballe, A. Kapitulnik, and S. S. Laderman, *Phys. Rev. B* **38**, 834 (1988).
- ³⁰Z. Z. Wang, J. Clayhold, N. P. Ong, J. M. Tarascon, L. H. Greene, W. R. McKinnon, and G. W. Hull, *Phys. Rev. B* **36**, 7222 (1987).
- ³¹Y. Lu, Y. F. Yan, H. M. Duan, L. Lu, and L. Li, *Phys. Rev. B* **39**, 729 (1989).
- ³²J. Clayhold, S. J. Hagen, N. P. Ong, J. M. Tarascon, and P. Barboux, *Phys. Rev. B* **39**, 7320 (1989).
- ³³Y. Koike, Y. Iwabuchi, S. Hosoya, N. Kobayashi, and T. Fukase, *Physica* **159C**, 105 (1989).
- ³⁴M. D. Kirk, J. Nogami, A. A. Baski, D. B. Mitzi, A. Kapitulnik, T. H. Geballe, and C. F. Quate, *Science* **242**, 1673 (1988).

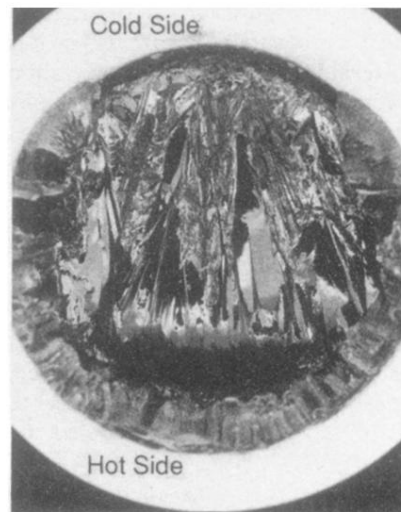


FIG. 1. Top view of an alumina crucible containing 2:2:1:2 crystals grown using a directional solidification approach. The crystals primarily nucleate on the cold side of the crucible and grow along the temperature gradient toward the hot side as the average temperature in the oven is reduced.